www.czasopisma.pan.pl PAN POLSKA AKADEMIA NAUK www.journals.pan.pl

Arch. Metall. Mater. **67** (2022), 4, 1243-1250

DOI: https://doi.org/10.24425/amm.2022.141048

A.-M. ROMAN[1], R. CHELARIU[1], R. CIMPOESU[1*], I. STIRBU[1], I. IONITA[1], M.M. CAZACU[2], B.A. PRISECARIU[3], N. CIMPOESU[3], P. PIETRUSIEWICZ[4], A. SODOR[3*]

ANALYSIS OF THE CORROSION RATE OF FeMn-Si BIODEGRADABLE MATERIAL

The Fe-based alloy with manganese led to the appearance of new austenitic alloys, with the antiferromagnetic property pursued, resulting in compatibility with the magnetic field as that of magnetic resonance imaging. The corrosion resistance behavior of the biodegradable Fe-Mn-Si alloy was analyzed in a thermostatic chamber at 37±1°C for 24, 48 and 72 hours by immersing in Ringer solution. Also, the cast and laminated samples were subjected to electro-corrosion tests using a potentiostat equipment. Linear and cyclic potentiometry is presented for characterize the corrosion behavior of the experimental samples in electrolyte. Due to the interaction between the alloy and the liquid medium a change in the solution pH was observed. Structure analysis and chemical composition details of the surfaces were obtained using electron scanning microscopy (SEM) and X-ray energy dispersive spectroscopy (EDS).

Keyword: Biodegradable; Fe-Mn alloy; Degradation Rate

1. Introduction

The idea of designing a biodegradable material for medical applications is a highly debated topic in the scientific world due to the mechanism of healing diseased tissue and subsequent degradation once its function is completed [1]. This process involves numerous aspects to be analyzed on the possible harmful effects on the human body due to the reactions that occur at the material/biological environment contact [2,3]. The corrosion rate and corrosion products released in the body can have effects on cytotoxicity and solution pH. It is desired to reach an optimal ratio between the rates of degradation/healing time through different methods of control over the properties of these biomaterials. The technology of obtaining the right materials for different types of implants [4] and the percentages of alloying elements in the chemical composition that are suitable for certain medical applications [5-7] represent a challenge for scientists. Mg-based alloys as biodegradable materials for medical implants have been considered for good biocompatibility and a relatively high rate of degradation compared to Fe-based alloys.

Fe-Mn alloys have been studied as biodegradable metals over time in various publications that have presented the possible advantages and disadvantages that they would have in the design of implants for cardiovascular [8] and orthopedic applications [9]. The low content of Mn element made possible the nontoxicity of biodegradable alloys [10] and showed good results regarding biocompatibility and mechanical properties. By adding new elements such as Si [11] the new biodegradable alloy with a shape memory effect showed a higher corrosion rate and mechanical properties superior to its predecessor Fe-Mn. Lower corrosion resistance was observed, due to the addition of Si, which increased the γ-austenite content [12]. Different alloying elements at different concentrations were used to study the biodegradability and biocompatibility of these alloys based on the Fe-Mn system [13].

Scientific papers published in the field show a great interest in the research of biodegradable alloys based on FeMn as biodegradable materials for implants. In vitro and in vivo tests have shown favorable results on degradation rate, mechanical properties and biocompatibility [14,15]. The shape memory effect that these types of alloys have, necessary for example, for pipe joints has been studied in terms of shape recovery characteristics in order to expand the range of applications for use [16]. FeMnSi-based alloys are being studied by researchers as an

[1] FACULTY OF MATERIALS SCIENCE AND ENGINEERING, "GHEORGHE ASACHI" TECHNICAL UNIVERSITY OF IASI, PROF.DR.DOC. D. MANGERON NO. 41 STREET, 700050 IASI, ROMANIA
[2] "GHEORGHE ASACHI" TECHNICAL UNIVERSITY OF IASI, DEPARTMENT OF PHYSICS, 700050 IASI, ROMANIA
[3] "GRIGORE T. POPA" UNIVERSITY OF MEDICINE AND PHARMACY OF IASI, 16 UNIV. STREET, 700115 IASI, ROMANIA
[4] CZĘSTOCHOWA UNIVERSITY OF TECHNOLOGY, DEPARTMENT OF PHYSICS, 42-200 CZĘSTOCHOWA, POLAND

* Corresponding author: amona.cimpoesu@tuiasi.ro

alternative to nitinol implants due to their lower cost and cold workability [17]. FeMnSi-Al alloys have the particularity of being SMA being studied in numerous specialized papers on transformation temperatures and deformation characteristics [18,19].

In this article, a new iron based shape memory alloy is proposed as biodegradable material. Corrosion and electrocorrosion results encouraged the application of this material for long term implants.

2. Materials and Methods

Two samples of the same FeMnSi-Al alloy were obtained for this work. One sample was obtained by casting from high purity Fe, master alloy FeMn and FeSi in an arc furnace and remelted five times for chemical and structural homogenization in induction furnace. The addition of aluminum was used to increase the degradation rate of the alloy subjected to the immersion environment and to change the transformation temperatures Ms-Mf, respectively As-Af, in order to obtain a good functionality of the material in the field of implants for medical applications. Second sample was in laminated state after rolling at 1100°C till 1mm thickness of the sample. All experiments were conducted in accordance to safety conditions regulations [20].

The surfaces were prepared for the tests with SiC metallographic paper, starting from 600 to 2400 grit. Before starting the experiment, the samples were cleaned in ultrasound bath with ethanol of 92% concentration and dried in air.

For the degradation tests, both samples were immersed in Ringer's solution (NaCl, KCl, $CaCl_2$, $NaHCO_3$ and $MgCl_2$) with a pH between 5.0-7.0 at a ratio of 20 ml/cm^2 [21,22] and incubated for 24, 48, and 72 h at a temperature of 37 ±1°C, respectively. After each immersion interval, the samples were extracted from the electrolyte solution and cleaned in an ultrasonic bath in ethyl alcohol solution. The corrosion compounds and the surface covered by them were subjected to chemical analysis, electronic and optical micrographs after each immersion interval mentioned above. The samples were weighed initially, after the immersion test and after ultrasonic cleaning to highlight the mass loss of the metallic material.

The electro-corrosion tests were performed in a three-electrode cell, with a platinum electrode as counter, an saturated calomel electrode as reference, and the samples with a area of 0,7 cm^2. All the experiments were performed in Ringer's solution at the 20°C temperature using an potentiostat PGP201. The liniar potentiodynamic polarization tests were done with a scanning rate of 1 mV/s and cyclic potentiodynamic polarization tests were done with a 10 mV/s scanning rate.

Chemical composition details of the surfaces were obtained using energy dispersive X-ray spectroscopy (EDS) Esprit PB-ZAF automated software and item list analyzed with Bruker detector connected to electron microscope scanning equipment (SEM) – VegaTescan LMH II (30 kV, SE detector, high vacuum).

3. Results and Discussion

Degradation Test

In the case of biodegradable alloys, variations in the mass of the experimental samples will always be observed following the interaction with an electrolyte solution because they interact a lot from the first contact. The degradation of materials is ensured by a continuous interaction between the sample and electrolyte medium even if these materials, similar to biocompatible, the surface passivation phenomenon occurs at some point in the interaction of the two media, the passivation layer does not have good stability on the surface, allowing the continuation of chemical interactions between the metal of the substrate and the electrolyte solution.

After 24 h of immersion in Ringer's solution, the samples showed an obvious increase in mass by the formation on the sample surface of oxides, chlorine-based compounds and carbonates (Eq. 1.3-1.6). After ultrasound cleaning of the surface and removal of unstable compounds from the surface of the experimental material, a decrease in the initial mass was observed. A larger amount of mass was lost in the case of the cast sample compared to the laminated one, which is in accordance with the literature on high corrosion rate of rolled samples compared to cast ones. After 48 h and 72 h from the beginning of the experiment, respectively, the samples decreased in mass, keeping the difference higher in the case of the cast sample. The corrosion rate according to mass loss was determined using the formula [23]:

$$CR = \frac{KW}{A\rho t} \tag{1.0}$$

Where: CR = corrosion rate [mm/Y]; $K = 8.76 \times 10^4$; W = weight loss = $Wf - Wi$ [g]; A = sample's initial area [cm^2]; ρ = material density [g/cm^3]; t = immersion time [h].

All corrosion rates calculated in this way are found in TABLE 1. The results show an increase proportional to the ex-

TABLE 1

Corrosion rate corresponding to mass loss

Sample	24 hours		48 hours		72 hours	
	Cast sample [C]	Laminated sample [L]	Cast sample [C]	Laminated sample [L]	Cast sample [C]	Laminated sample [L]
Initial mass [mg]	4164.3	774.6	4139.7	758.9	4002.8	739.2
Mass after immersion [mg]	4164.7(+0.4)	775.1(+0.5)	4139.0(–0.7)	758.7(–0.2)	4002.7(–0.1)	739.1(–0.1)
Mass after ultrasonic cleaning [mg]	4163.7(–0.6)	774.3(–0.3)	4137.7(–2.0)	757.8(–1.1)	3999.9(–2.9)	736.7(–2.5)
Corrosion rate [mm/Y]	0,084	0,053	0,14	0,096	0,135	0,146

posure time of the samples to the electrolyte medium, the highest corrosion rate was recorded on the laminated sample, 72 h after immersion. The differences in rate between the first days is given by the chemical reactions that occur at the contact of the alloy with the Ringer solution.

In the first 24 hours, based mainly on formation of ferrous oxides, an increase of the mass is observed in both cases melted and laminated. After ultrasound cleaning, a part of these compounds, with no more stability on the surface, pass to electrolyte solution decreasing the sample mass. After 48 and 72 hours no more gain in mass was observed for all experimental samples, TABLE 1, all of them presenting a loss of mass. In the first hours laminated sample present a better corrosion resistance in electrolyte and after 48 hours and the surface layers were removed the melted and laminated samples changed the resistance to corrosion values.

Dispersive X-ray Spectroscopy (EDX) Results

Chemical composition details were obtained using energy dispersive X-ray spectroscopy (EDX) and the list of items analyzed with the mode detector connected to the electron microscope scanning equipment (SEM). Standard deviations were provided for all chemical determination. The analysis was performed in various areas on the surface of the material (1 mm^2) and an average was made. Initially (TABLE 2) it is observed the identification of the basic elements: Fe, Mn, Si and Al at different X-ray energies for the elements iron and manganese. The chemical composition is proper for shape memory effect and addition of Al was realized in order to modify the solid-state transformation temperatures of austenite to martensite and reverse [24-26].

TABLE 2

Chemical composition of the experimental alloy in its initial state

Elements	Fe		Mn		Si		Al	
Sample	Wt%	At%	Wt%	At%	Wt%	At%	Wt%	At%
Cast	78.90	73.76	14.53	13.81	3.47	6.45	3.09	5.98
Laminated	81.18	77.18	13.99	13.52	2.86	5.41	1.97	3.89
EDS error	2.06		0.46		0.25		0.25	

Standard deviation (made on 20 determinations): Fe:±1, Mn:±0.25, Si:±0.1 and Al:±0.1

The differences between melted and laminated samples in chemical composition appear, at least at the surface (>5 μm) during the loss of silicon and aluminum elements on the rolling process.

After contact with Ringer electrolyte solution for 24 h, additional surface identification of the elements is observed: oxygen, carbon, chlorine and sodium (TABLE 3). After 48 h, the analysis showed in the composition the presence of potassium and calcium in small quantities. In this case, the bioactivity specific to orthopedic applications could be shown by the precipitation reaction of Ca/P [27]. After ultrasonic cleaning in technical alcohol, the disappearance of sodium, potassium and calcium from the surface and maintenance of oxygen, carbon and chlorine is observed. Tab. 3 presents the results of chemical analyzes performed on the surface of the rolled and cast experimental alloy before and after immersion in Ringer electrolyte solution, respectively after ultrasonic cleaning in technical alcohol for 24, 48, and 72 h. From the electrolyte solution, compounds based on carbon, oxygen, sodium and chlorine passed on the surface of the experimental alloy. The vast majority of compounds are oxygen-based (with a percentage of 34 wt. %) of which after

TABLE 3

Chemical composition obtained after each immersion test and after cleaning in an ultrasonic bath

Elements/ samples (C:cast, L:laminated, I: after immersion, I+UC: after immersion and ultrasonic cleaning)			Fe		Mn		Si		Al		O		C		Cl		Na		K		Ca	
			wt%	at%	wt%	at%	wt%	at%	wt%	at%	wt%	at%	wt%	at%	wt%	at%	wt%	at%	wt%	at%	wt%	at%
24 h	C	I	47.80	21.96	6.93	3.24	1.50	1.37	1.73	1.65	29.90	47.96	10.19	21.77	0.29	0.21	1.65	1.85	—	—	—	—
		I+UC	49.85	23.52	8.88	4.26	1.61	1.51	2.02	1.98	22.84	37.63	13.63	29.90	0.33	0.25	0.83	0.95	—	—	—	—
	L	I	48.30	21.85	5.61	2.58	1.25	1.13	1.25	1.17	32.66	51.58	9.86	20.73	0.53	0.38	0.54	0.59	—	—	—	—
		I+UC	50.35	23.61	8.21	3.91	2.09	1.95	1.94	1.88	23.32	38.15	13.94	30.39	0.15	0.11	—	—	—	—	—	—
48 h	C	I	52.52	28.66	9.79	5.43	1.74	1.88	1.70	1.92	26.34	50.18	1.76	4.47	1.34	1.15	4.67	6.19	0.06	0.05	0.09	0.07
		I+UC	49.19	23.73	9.14	4.48	1.76	1.69	1.83	1.82	25.76	43.37	10.12	22.71	0.93	0.71	1.27	1.49	—	—	—	—
	L	I	47.25	21.91	5.52	2.60	1.58	1.46	1.70	1.63	34.11	55.22	6.63	14.29	1.76	1.29	1.39	1.57	0.05	0.04	—	—
		I+UC	45.03	20.29	7.34	3.36	2.02	1.81	2.03	1.89	30.19	47.48	10.81	22.66	0.80	0.57	1.78	1.95	—	—	—	—
72 h	C	I	43.91	19.41	7.87	3.53	1.09	0.96	0.86	0.79	34.33	52.96	9.89	20.32	0.39	0.27	1.61	1.73	0.05	0.03	—	—
		I+UC	47.77	21.97	8.75	4.09	1.35	1.23	1.61	1.53	29.06	46.64	11.48	24.55	—	—	—	—	—	—	—	—
	L	I	53.30	28.10	7.30	3.91	2.03	2.13	2.54	2.78	33.17	61.05	9.67	21.40	—	—	1.32	1.69	0.06	0.04	0.06	0.05
		I+UC	39.09	18.61	6.36	3.08	1.96	1.86	2.50	2.46	30.26	50.31	—	—	—	—	—	—	—	—	—	—
EDS error			1.57		0.35		0.18		0,18		4.09		4.33		0.08		0.19		0,04		0,05	
St. Dev (made on 20 determinations) of: Fe: ±1, Mn: ±0.7, Si: ±0.41, Al: ±0.3, O: ±1.2, C: ±0.7, Cl: ±0.1,Na: ±0.1, K: ±0.1, Ca: ±0.2																						

ultrasonic cleaning about 10 wt. % are lost by detaching from the surface and passing into the cleaning solution. Carbonates had higher stability, the increased percentage of carbon after the cleaning operation was due to the decrease in the oxygen percentage. After the immersion test, the appearance of salts on the surface was observed. Sodium chloride compounds passed into the solution after the cleaning stage without stability on the metal surface. Following the cleaning step, no compounds based on sodium, calcium and potassium were identified and only traces of chlorites remained on the surface. In the last cleaning stage at the end of the experiment, only the presence of oxides was registered, the other compounds being removed in the case of the laminated sample.

Electro-Corrosion Test

Experimental results registered with the potentiostat equipment for both experimental samples are presented in TABLE 4. The cast state sample has the highest corrosion current and the highest polarization resistance value that will accelerate the degradation rate of the material. Both the anodic and cathodic branches are similar, so reduction and oxidation reactions occur during the electro-corrosion experiment. Based on the corrosion rate determined the alloys can be proposed for different medical applications to fulfill the degradation rate.

TABLE 4

Electro-corrosion process parameters

Sample	E_0 [mV]	b_a [mV]	b_c [mV]	R_p [ohm.cm²]	J_{corr} [mA/cm²]	V_{corr} [µm/Y]
Cast	–1071.0	–81.0	87.3	90.82	38.2939	430.0
Laminated	–1164.0	–75.0	83.8	224	5.4294	60.97

Linear Tafel curves (Fig. 1a) show the variation of the corrosion current with modification of the experiment potential. The highest corrosion resistance is of the laminated sample and the differences between samples is not very big being in 100 mV. Both anodic and cathodic branches are appropriate highlighting the fact that oxidation and reduction take place on the surface of the experimental alloys. As for cyclic potentiometry (Fig. 1b), the general corrosion characteristics of the experimental samples behavior in Ringer's solution are noticed. The cast sample present a higher current density, (Fig. 1b) and small variations based on local accelerated corrosion (based on inclusions or bigger pores etc.). Pores, cracks, micro-cracks and chemical inhomogeneity (Fig. 2a) presented by the cast sample caused variations in current density. No passivation process was registered for these samples based on the continuous degradation of the sample surface and insignificant periods of passivation after the iron oxide formation, to be reduced as time maintaining to be represented on the graph, followed by the fast penetration of the passivation layer and the continuing degradation of the material through corrosion.

PH Monitoring

During the experiment, the solution changed its pH value in both cases (Fig. 3). The pH-meter recorded values for 0-24 h, 24-48 h, and 48-72 h. The cast material (Fig. 3a) behaves in the same way as the laminated one (Fig. 3b) with a higher increase in the pH values after 2500 min to values of 7.5 passing from the acidic environment to the basic one. The cast sample registered different reactions, after 2500 min, with a pH increasing from relatively stabilized values between 6.2-6.4 to values above 7. This can be associated with the formation of goethite (α-FeOOH) and the formation of a small amount of Ca based compounds [28] detected according to the EDS analysis at 72 h. The pH decreases, from 24-48 h in the case of the laminated sample due to the formation of free acid (Eq. 1.6), mainly due to pitting marks at the surface of the metallic material. These fluctuations in the basicity/acidity of the electrolyte solution occur throughout all analyzed period (72 h). Both experimental samples registered these fluctuations, due to the alternation of reactions that occur on the surface of the material and depending on the areas where they occur at a different time.

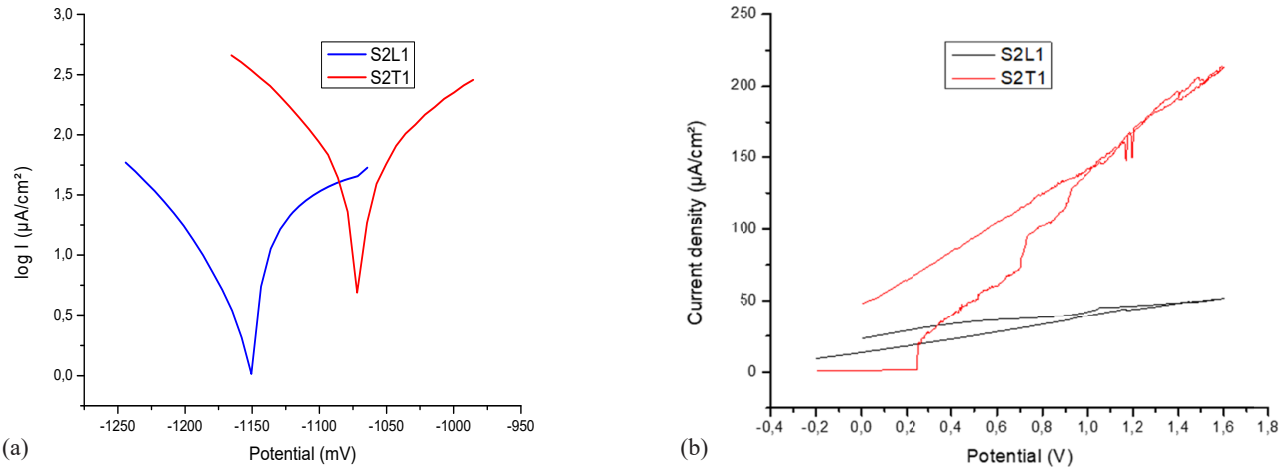

Fig. 1. Tafel diagrams of the experimental alloy: (a) linear and (b) cyclic potentiometry; (S2T-cast sample, S2L-laminated sample)

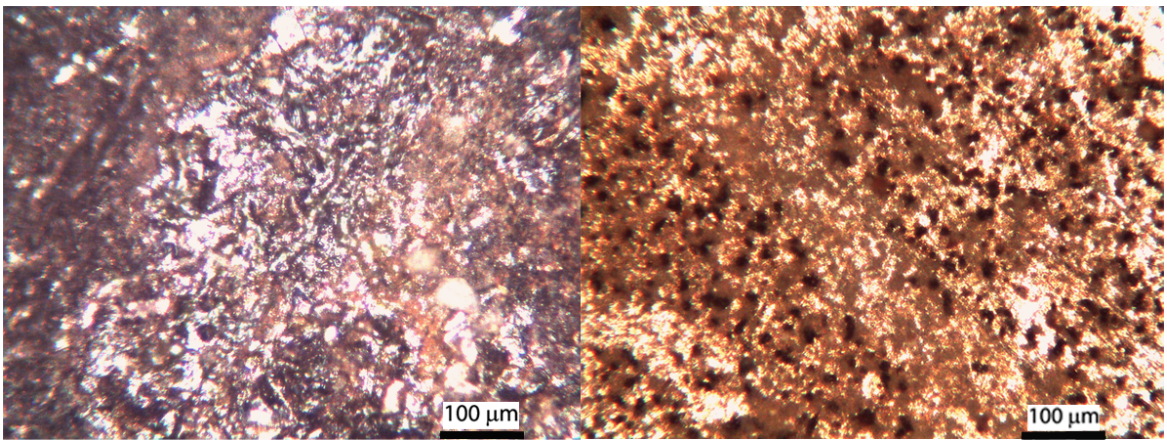

(a) (b)

Fig. 2. Optical micrographs after the electro-corrosion process for: (a) cast sample; (b) laminated sample

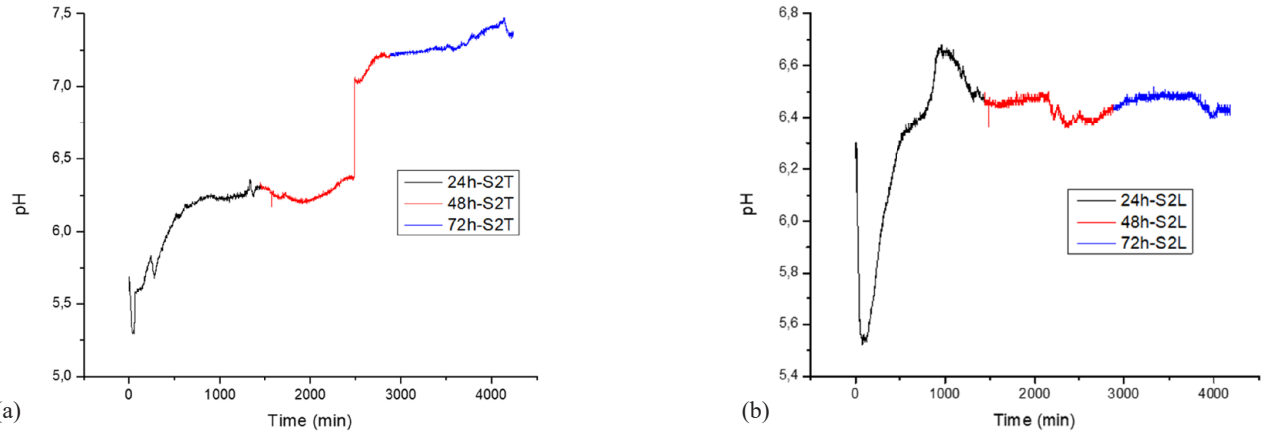

(a) (b)

Fig. 3. The pH variation registered for the experimental samples during 3 days of immersion test: (a) cast; (b) laminated

The pH variations monitoring over experiments provided information about the time of corrosion compounds formation at the electrolyte/biomaterial interface [29]:

Anodic reaction:

$$Fe \rightarrow Fe^{2+} + 2e^{-} \quad (1.1)$$

$$Mn \rightarrow Mn^{2+} + 2e^{-}$$

Cathodic reaction:

$$1/2O_2 + H_2O + 2e^{-} \rightarrow 2HO^{-} \quad (1.2)$$

Compound formation and dissolution:

$$Fe^{2+} + 2HO^{-} \rightarrow Fe(HO)_2(s) \quad (1.3)$$

$$2Fe(HO)_2(s) + H_2O + 1/2O_2 \rightarrow 2Fe(HO)_3(s) \quad (1.4)$$

$$Fe^{2+} + 2Cl^{-} \rightarrow FeCl_2 \quad (1.5)$$

$$FeCl_2 + 2H_2O \rightarrow Fe(HO)_2 + 2H^{+} + Cl^{-} \quad (1.6)$$

$$Fe^{2+} + CO_3^{2-} \rightarrow FeCO_3(s) \quad (1.7)$$

The further production of insoluble compounds $Fe(HO)_2$ (s) is done by the reaction between the released Fe^{2+} ions and HO^{-} (Eq. 1.3). Hydroxo-polymers and oxyhydroxides as well as Fe-complexes are formed together with $Fe(HO)_3$ (Eq. 1.4). The prevalence of Fe-complexes depends on the pH value [30]. Aggressive Cl ions present on the surface of the material activate the degradation process (Eq. 1.5). Water hydrolysis and the formation of free acid (Eq. 1.6) will lead to localized corrosion on the metal surface. Further carbonates will lead to the formation of insoluble compounds (Eq. 1.7). Studies addressing the biocompatibility of biomaterials report that cytotoxicity should be analyzed in the following reactions that contribute to changes in pH in solution due to insoluble corrosion products [31].

Surface characterization through *Scanning Electron Microscopy* (SEM)

Electron microscopy of the surface shows the formation of corrosion compounds (Fig. 4a-h). After 48 h of immersion test, the cast sample shows clear traces of cracks (Fig. 4b). Respectively after 72 h cracks and crystals of different sizes distributed over the entire surface were observed (Fig. 4c), these were present in a smaller amount after ultrasonic cleaning. The compounds are based on oxides and hydroxides of iron and manganese, as well as silicon and aluminum in smaller quantities, but on carbonates, salts or chlorates, which were formed because of the interaction

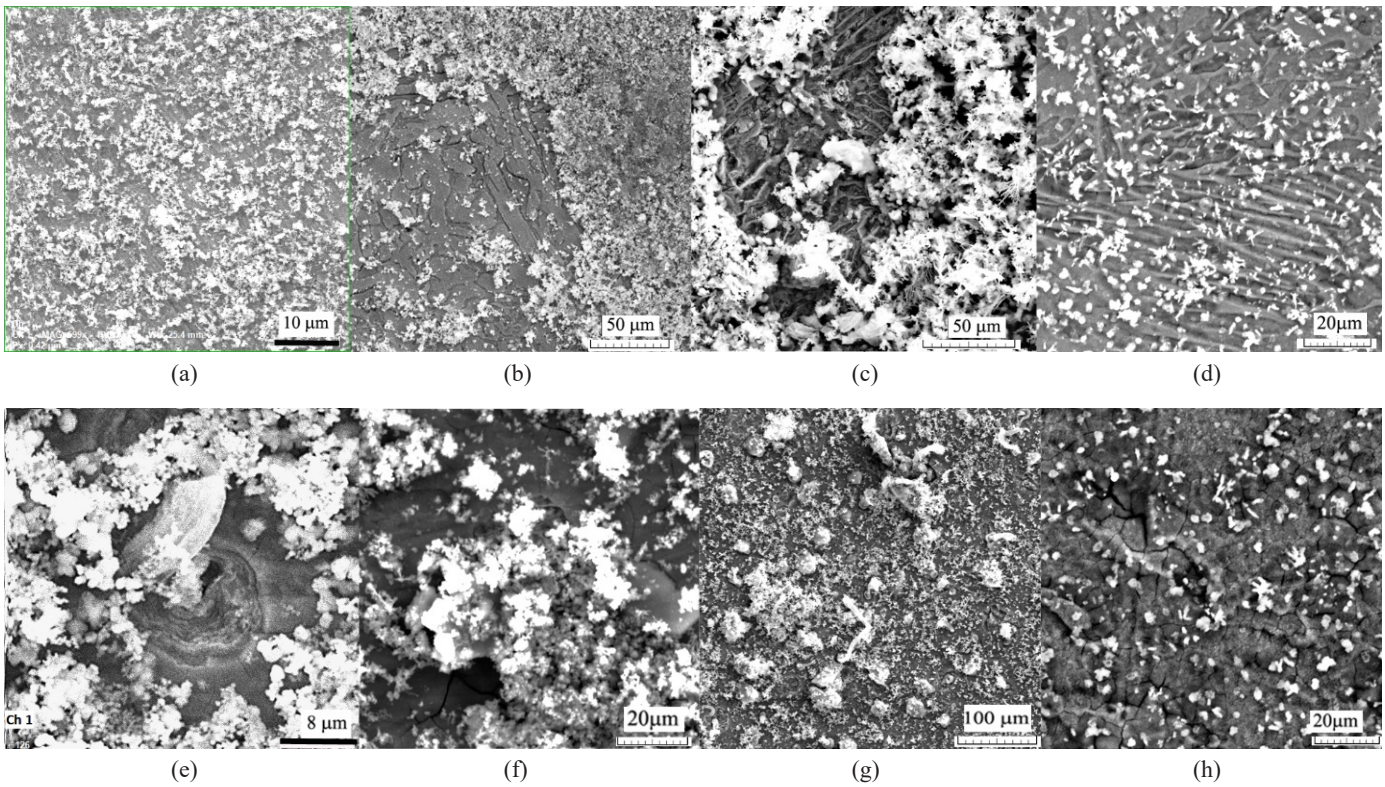

Fig. 4. SEM micrographs for the cast sample: (a) after 24 h of immersion; (b) after 48 h of immersion; (c) after 72 h of immersion; (d) after ultrasonic cleaning the 72 h-immersed sample, and the laminated one: (e) after 24h of immersion; (f) after 48 h of immersion; (g) after 72 h of immersion; (h) after ultrasonic cleaning the 48 h-immersed sample

between experimental and electrolyte environment. Analyzing Fig. 4e), the laminated sample also underwent a chemical attack of pitting type with pits around 10 µm in diameter in which a layered corrosion of the material is observed. The compounds formed on the metal surface have a porous structure (Fig. 4f, g), with oxides of all elements that make up the alloy and compounds based on carbon, chlorine and sodium. A substantial part of the compounds was removed after ultrasound cleaning from the surface of the 72 h immersed laminated sample (Fig. 4h). The removal was for those who does not have good stability and only that part which is bonded to the surface of the alloy by various chemical reactions remained. The signal of iron and manganese is masked by oxides that have remained attached to the metal surface. They will contribute over time, if contact with the electrolyte solution is maintained, to the general degradation of the material. In addition to the more pronounced pitting traces after 72 h, cracks of the formed oxide layer are observed on the metallic material of the laminated sample, defects that contribute to the detachment of the substrate material.

Surface characterization through *Optical Microscopy* (OM)

The surfaces of the experimental alloys were analyzed using an optical microscope (Fig. 5) to highlight the corrosion details. Following the visual observations on the experimental specimens FeMnSi-Al, the appearance of some compounds on the surface as well as the traces of corrosion are observed. The compounds, partially hydroxides, appeared as a red-brown surface layer on the top, which proves the presence of anti-ferromagnetic hematite (α-Fe2O3) on the surface, gray with shades of wüstite green (FeO) and a black layer on the surface as magnetite (Fe3O4). After ultrasound, traces of corrosion appeared on the cast sample (Fig. 5b). They are distributed over the entire surface compared to the laminated one (Fig. 5d), which has a non-uniform morphology with uneven pitting pits.

4. Conclusions

A new shape memory alloy material FeMnSi with addition of Al was made through arc melting and induction vacuum remelting. The material under study showed good biodegradability properties and can be considered a candidate for implants in medical applications. All samples showed a decrease in mass after 72 h of immersion in SBF due to degradation of the material in the electrolyte solution by oxidation for the most part. The interaction between the alloy and the liquid medium changes the pH of the solution over time. Microstructurally and chemically, a partial removal of the compounds was observed after ultrasonic cleaning, especially of the salts that passed from the surface into the solution. A pitting corrosion was observed under the layer of compounds and multiple cracks and crevices. Of course, a repetition of the experiment is required for a longer study to follow the repeatability of the material's behavior.

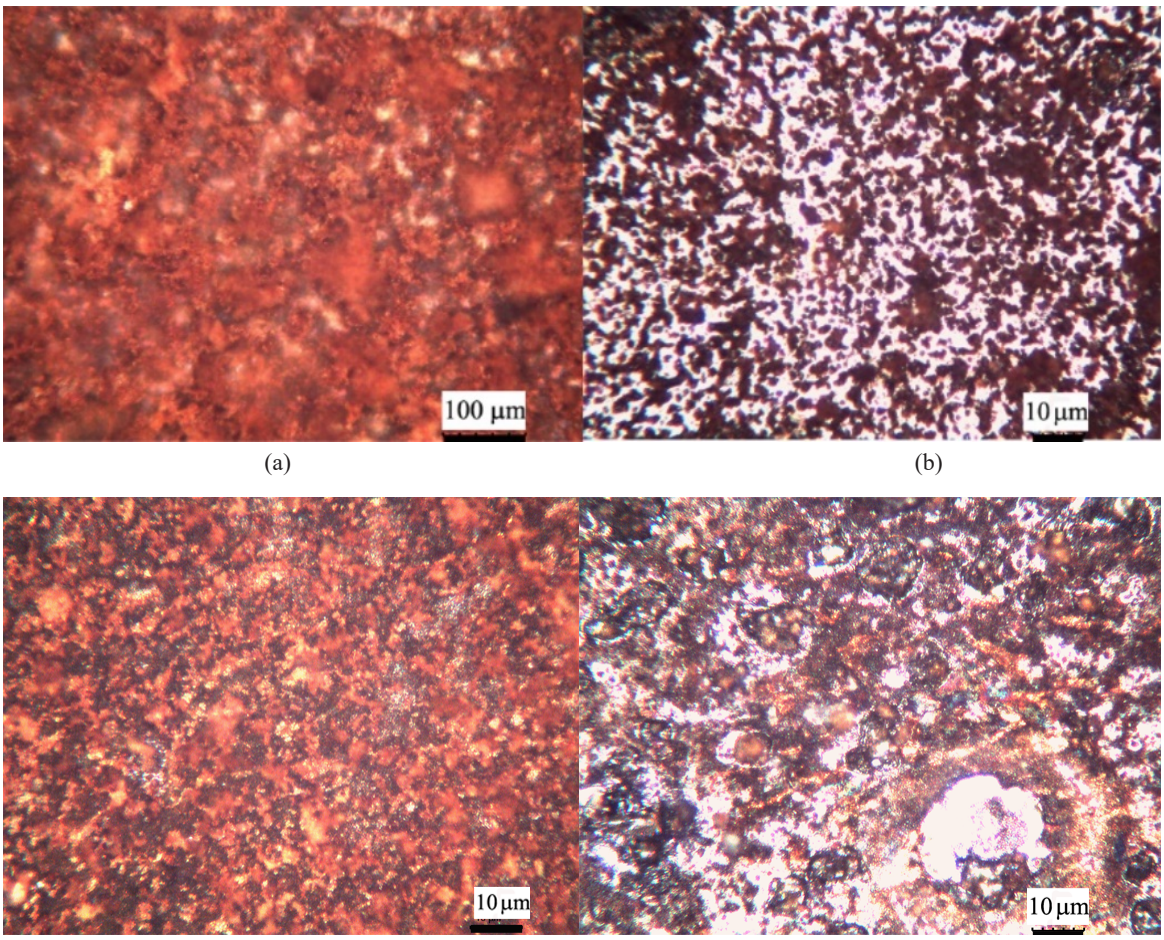

Fig. 5. Optical micrographs after 72 h of immersion test: (a) cast, (c) laminated; and after the ultrasonic cleaning stage: (b) cast, (d) laminated

Acknowledgments

This work was supported by a grant of the Romanian Ministry of Education and Research, CNCS – UEFISCDI, project number PN-III-P1-1.1-TE-2019-1921, within PNCDI III.

REFERENCES

[1] H. Hermawan, D. Dubé, D. Mantovani, Development of Degradable Fe-35Mn Alloy for Biomedical Application, Mater. Sci. Eng. **15-17**, 107-112 (2007). DOI: https://doi.org/10.4028/www.scientific.net/AMR.15-17.107

[2] M. Schinhammer, A.C. Hänzi, J.F. Löffler, P.J. Uggowitzer, Design Strategy for Biodegradable Fe-Based Alloys for Medical Applications, Acta Biomater. **6** (5), 1705-1713 (2010). DOI: https://doi.org/10.1016/j.actbio.2009.07.039

[3] D. Spandana, H. Desai, D. Chakravarty, R. Vijay, K. Hembram, Fabrication of a biodegradable Fe-Mn-Si alloy by field assisted sintering, Adv. Powder Technol. **31**, 4577-4584 (2020). DOI: https://doi.org/10.1016/j.apt.2020.10.012

[4] M.S. Baltatu, P. Vizureanu, A.V. Sandu, C. Munteanu, B. Istrate, Microstructural Analysis and Tribological Behavior of Ti-Based Alloys with a Ceramic Layer Using the Thermal Spray Method, Coatings **10** (12), 1216 (2020). DOI: https://doi.org/10.3390/coatings10121216

[5] A.V. Sandu, M.S. Baltatu, M. Nabialek, A. Savin, P. Vizureanu, Characterization and Mechanical Proprieties of New TiMo Alloys Used for Medical Applications, Materials **12** (18), 2973 (2019). DOI: https://doi.org/10.3390/ma12182973

[6] B. Istrate, C. Munteanu, S. Lupescu, R. Chelariu, M.D. Vlad, P. Vizureanu, Electrochemical Analysis and In Vitro Assay of Mg-0.5Ca-xY Biodegradable Alloys, Materials **13** (14), 3082 (2020). DOI: https://doi.org/10.3390/ma13143082

[7] C. Panaghie, R. Cimpoesu, A. Alexandru, M. Bernevig, V. Manole, A.M. Roman, B.A. Prisacariu, P. Paraschiv, N. Cimpoesu, Chemical and structural analyze of experimental biodegradable ZnMgY alloy, Mater. Sci. Eng. **1037**, 012034 (2021). DOI: https://doi.org/10.1088/1757-899X/1037/1/012034

[8] H. Hermawan, A. Purnama, D. Dube, J. Couet, D. Mantovani, Fe-Mn alloys for metallic biodegradable stents: Degradation and cell viability studies, Acta Biomater. **6** (5), 1852-1860 (2010). DOI: https://doi.org/10.1016/j.actbio.2009.11.025.

[9] Y. Nie, G. Chen, H. Peng, S. Tang, Z. Zhou, F. Pei, B. Shen, In vitro and 48 weeks in vivo performances of 3D printed porous Fe-30Mn biodegradable scaffolds, Acta Biomater. **121**, 724-740 (2021). DOI: https://doi.org/10.1016/j.actbio.2020.12.028

[10] A. Drynda, T. Hassel, F.W. Bach, M. Peuster, In vitro and in vivo corrosion properties of new iron-manganese alloys designed for cardiovascular applications, J. Biomed. Mater. Res. B. **103** (3), 649-660 (2015). DOI: https://doi.org/10.1002/jbm.b.33234

[11] B. Liu, Y.F. Zheng, L. Ruan, In vitro investigation of Fe30Mn6Si shape memory alloy as potential biodegradable metallic material, Mater. Lett. **65** (3), 540-543 (2011). DOI: https://doi.org/10.1016/j.matlet.2010.10.068

[12] H.C. Lin, K.M. Lin, C.S. Lin, T.M. Ouyang, The corrosion behavior of Fe-based shape memory alloys, Corros. Sci. **44** (9), 2013-26 (2002). DOI: https://doi.org/10.1016/s0010-938X(02)00027-6

[13] B. Liu, Y.F. Zheng, Effects of alloying elements (Mn, Co, Al, W, Sn, B, C and S) on biodegradability and in vitro biocompatibility of pure iron, Acta Biomater. **7** (3), 1407-1420 (2011). DOI: https://doi.org/10.1016/j.actbio.2010.11.001

[14] M. Peuster, P. Wohlsein, M. Brügmann, M. Ehlerding, K. Seidler, C. Fink, H. Brauer, A. Fischer, G. Hausdorf, A novel approach to temporary stenting: degradable cardiovascular stents produced from corrodible metal-results 6-18 months after implantation into New Zealand white rabbits, Heart **86**, 563-569 (2001).

[15] T. Kraus, F. Moszner, S. Fischerauer, M. Fiedler, E. Martinelli, J. Eichler, F. Witte, E. Willbold, M. Schinhammer, M. Meischel, P.J. Uggowitzer, J.F. Löffler, A. Weinberg, Biodegradable Fe-based alloys for use in osteosynthesis: Outcome of an in vivo study after 52 weeks, Acta Biomater. **10**, 3346-3353 (2014).

[16] M. Wada, H. Naoi, H. Yasuda, T. Maruyama, Shape recovery characteristics of biaxially prestrained Fe-Mn-Si-based shape memory alloy, Mater. Sci. Eng. A **481-482**, 178-182 (2008).

[17] R.A. Rahman, D. Juhre, T. Halle, S. Mehmood, W. Asghar, Types, DSC Thermal Characterization of Fe-Mn-Si based Shape Memory Smart Materials and their Feasibility for Human Body in Terms of Austenitic Start Temperatures, J. Eng. Technol. **8** (1), 185-206 (2019).

[18] M. Koyama, T. Sawaguchi, K. Ogawa, T. Kikuchi, M. Murakami, The effects of thermomechanical training treatment on the deformation characteristics of Fe-Mn-Si-Al alloys, Mater. Sci. Eng. A **497**, 353-357 (2008).

[19] Y.H. Wen, H.B. Peng, D. Raabe, I. Gutierrez-Urrutia, J. Chen, Y.Y. Du, Large recovery strain in Fe-Mn-Si-based shape memory steels obtained by engineering annealing twin boundaries, Nat. Commun. **5**, 4964 (2014).

[20] M.A. Bernevig-Sava, D.C. Darabont, M. Lohan, E. Mihalache, C. Bejinariu, Selection and verification of personal protective equipment in the context of current legal requirements, Quality-Access to Success **20**, 109-112 (2019).

[21] Y. Li, J. Yan, W. Zhou, P. Xiong, P. Wang, W. Yuan, Y. Zheng, Y. Cheng, In vitro degradation and biocompatibility evaluation of typical biodegradable metals (Mg/Zn/Fe) for the application of tracheobronchial stenosis, Bioact. Mater. **4**, 114-119 (2019). DOI: https://doi.org/10.1016/j.bioactmat.2019.01.001

[22] N. Cimpoesu, F. Sandulache, B. Istrate, R. Cimpoesu, G. Zegan, Electrochemical Behavior of Biodegradable FeMnSi-MgCa Alloy, Metals **8** (7), 541 (2018). DOI: https://doi.org/10.3390/met8070541

[23] P. Nayak, A.K. Biswal, S.K. Sahoo, Processing and characterization of Fe-35Mn biodegradable metallic materials, Mater. Today Proc. **33** (8), 5284-5289 (2020). DOI: https://doi.org/10.1016/j.matpr.2020.02.966

[24] B. Pricop, A.U. Soyler, B. Ozkal, L.G. Bujoreanu, Powder Metallurgy: An Alternative for FeMnSiCrNi Shape Memory Alloys Processing, Front. Mater. **7**, 247 (2020). DOI: https://doi.org/10.3389/fmats.2020.00247

[25] M. Popa, E. Mihalache, V.D. Cojocaru, C. Gurau, G. Gurau, N. Cimpoesu, B. Pricop, R.I. Comaneci, M. Vollmer, P. Krooss, T. Niendorf, L.G. Bujoreanu, Effects of Thermomechanical Processing on the Microstructure and Mechanical Properties of Fe-Based Alloys, J. Mater. Eng. Perform. **29** (4), 2274-2282 (2020). DOI: https://doi.org/10.1007/s11665-020-04609-z

[26] L.G. Bujoreanu, Development of shape memory and superelastic applications of some experimental alloys, J. Optoelectron. Adv. M. **17** (9-10), 1437-1443 (2015).

[27] H. Dong, F. Lin, A.R. Boccaccini, S. Virtanen, Corrosion behavior of biodegradable metals in two different simulated physiological solutions: Comparison of Mg, Zn and Fe, Corros. Sci. **182**, 109278 (2021). DOI: https://doi.org/10.1016/j.corsci.2021.109278

[28] E. Mouzou, C. Paternoster, R. Tolouei, A. Purnama, P. Chevallier, D. Dubé, F. Prima, D. Mantovani, In vitro degradation behavior of Fe-20Mn-1.2C alloy in three different pseudo-physiological solutions, Mater. Sci. Eng. C Mater. Biol. Appl. **61**, 564-573 (2016). DOI: https://doi.org/10.1016/j.msec.2015.12.092

[29] M. Moravej, A. Purnama, M. Fiset, J. Couet, D. Mantovani, Electroformed pure iron as a new biomaterial for degradable stents: in vitro degradation and preliminary cell viability studies, Acta Biomater. **6** (5), 1843-1851 (2010). DOI: https://doi.org/10.1016/j.actbio.2010.01.008

[30] M. Pivokonsky, J. Safarikova, P. Bubakova, L. Pivokonska, Coagulation of peptides and proteins produced by Microcystis aeruginosa: Interaction mechanisms and the effect of Fe-peptide/protein complexes formation, Water Res. **46** (17), 5583-5590 (2012). DOI: https://doi.org/10.1016/j.watres.2012.07.040

[31] N.S. Fagalia, C.A. Grilloa, S. Puntarulo, M.A. Fernández Lorenzo de Melea, Cytotoxicity of corrosion products of degradable Fe-based stents: Relevance of pH and insoluble products, Colloid. Surface. B **128**, 480-488 (2015). DOI: https://doi.org/10.1016/j.colsurfb.2015.02.047.